Rescuing *Chlamydomonas* motility in mutants modeling spermatogenic failure

We used *Chlamydomonas reinhardtii* motility mutants with disrupted genes homologous to human SPEF2 or DNALI1 to model spermatogenic failure disorders SPGF43 and SPGF83, respectively. We recovered aspects of wild-type motility in these mutants with a small-scale drug screen.

Version 4, published Dec 12, 2025. Originally published Dec 14, 2024.

Arcadia Science DOI: 10.57844/arcadia-fe2a-711e

Purpose

Spermatogenic failure (SPGF) is a significant cause of male infertility. This study addresses the challenges in studying SPGF43 and SPGF83, specific subtypes of SPGF with no known treatment, caused by mutations in the *SPEF2* and *DNALI1* genes, respectively.

Given the difficulty in obtaining human sperm samples with these specific genetic mutations, we studied these diseases using *Chlamydomonas reinhardtii* mutants with similar genetic defects and exhibiting similar motility phenotypes. We determined whether compounds that increase human sperm motility can restore normal motility in the *C. reinhardtii* mutant strains modeling SPGF as a method to discover novel treatments for this disease.

This work provides the community with a validated model system and screening methodology that can be expanded to test large chemical libraries or adapted to study other forms of genetic male infertility. For clinicians and pharmaceutical researchers, our findings demonstrate the potential of using *C. reinhardtii* as a rapid, cost-effective first-line screening tool before advancing promising compounds to more resource-intensive human studies. Additionally, our results

suggest specific molecular pathways that could be targeted in future drug development efforts for SPGF43 and SPGF83 treatment.

- This pub is part of the **platform effort**, "Genetics: Decoding evolutionary drivers across biology." Visit the platform narrative for more background and context.
- All associated **code** is available in this GitHub repository.
- **Data** from this pub, including raw and processed microscopy data and the coordinates from our cell tracking, is available from the BioImage Archive [1]. Additional, processed data is available in the GitHub repo.

We've put this effort on ice!

Background and goals

Infertility impacts one in six adults [2], and up to half of these cases are caused by spermatogenic failure (SPGF) resulting from mutations in single genes [3]. SPGF can present as loss of sperm production (azoospermia), low sperm counts (oligozoospermia), low sperm motility (asthenozoospermia), altered sperm morphology (teratozoospermia), or a combination of indications [4]. Although SPGF is common, it's challenging to study. The gene causing SPGF in a specific case is frequently unknown; thus, SPGF sperm samples with known mutations are challenging to acquire. We used a recently published dataset from a phylogenetic analysis using NovelTree [5][6] to identify organisms with genes that, while controlling for shared evolutionary history, are highly homologous in sequence and structure to the proteins encoded by human *SPEF2* (sperm flagellar 2) and *DNALI1* (dynein axonemal light intermediate chain 1). Loss-of-function mutations in *SPEF2* and *DNALI1* cause spermatogenic failure disorders known as SPGF43 and SPGF83, respectively.

SPGF43 and SPGF83 share similar behavioral and structural phenotypes despite being caused by distinct mutations. First reported in 2019, *SPEF2* mutations result in 0–0.6% sperm motility and 1–35% normal flagellar morphology [7][8]. Structural

analysis revealed severely disorganized axonemes in sperm flagellum [9]. Similarly, the *DNALI1* mutation was identified in 2023 in a patient with 0% motility and 47% normal flagellar morphology. Structural analysis showed asymmetric fibrous sheaths and missing inner dynein arm components [10].

Several studies have aimed to characterize SPGF43 and SPGF83 in mouse models and found that, in addition to SPGF-like phenotypes, loss-of-function mutations in either *SPEF2* or *DNALI1* causes hydrocephalus in these animal models [11][10], complicating experiments. This off-target and extreme phenotype has been avoided by generating germline-specific *SPEF2* or *DNALI1* knockouts [12][13]. These studies have provided valuable insights into the composition and structure of SPGF mouse sperm.

We recently developed a quantitative framework to identify unexpected model organisms for studying human biology by analyzing protein conservation patterns across 63 diverse eukaryotes. This framework challenges traditional assumptions about which species are "best" for modeling specific human traits [6]. We used this framework to determine the “best” organisms to model SPGF43 and SPGF83, revealing multiple organisms that ranked “better” than mice to model these diseases (Figure 1).

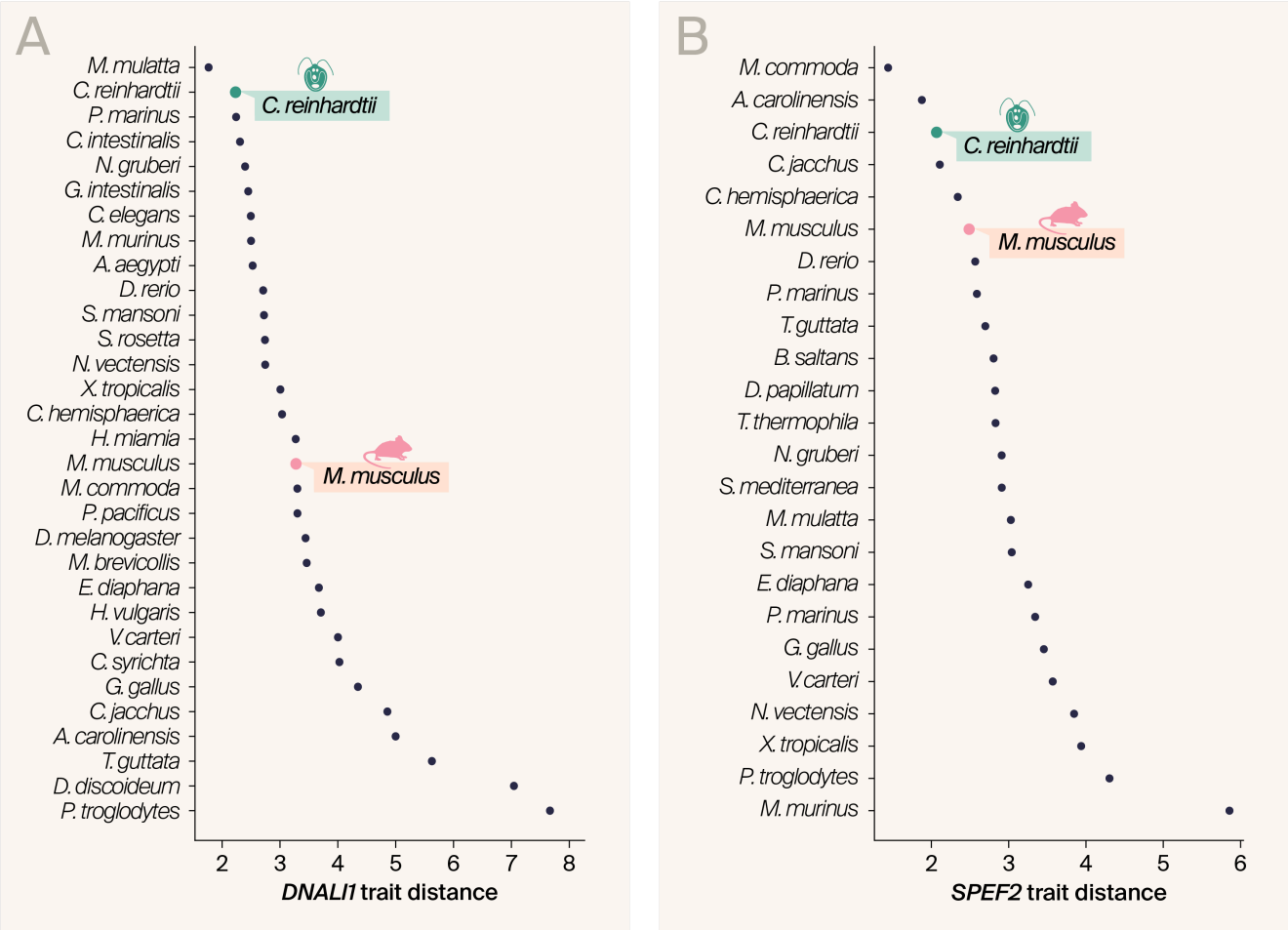

Figure 1. **Organism relevance to model SPGF43 and SPGF83**.

Physicochemical trait distances (td) between non-human species and *Homo sapiens* orthologs for *DNALI1* (A) and *SPEF2* (B). Only species with single-copy orthologs are shown. A smaller trait distance indicates a greater physicochemical similarity to the human protein when corrected for phylogeny. *Chlamydomonas* has a smaller trait distance than *Mus musculus* for both *DNALI1* ($td_{Chlamydomonas}$ = 2.23 [p = 0.09]; td*Mus* = 3.28 [p = 0.51]) and *SPEF2* ($td_{Chlamydomonas}$ = 2.06 [p = 0.05]; td_{Mus} = 2.48 [p = 0.12]) when compared to humans.

We decided to use *Chlamydomonas reinhardtii* to model these diseases for multiple reasons. First, we identified *C. reinhardtii* as a suitable organism to model multiple SPGF disorders using our phylogenetically corrected structure and sequence analysis (Figure 1). Second, *C. reinhardtii* and human sperm swim using similarly structured flagella [14][15] (Figure 2). Third, decades before the characterization of SPG43 and SPGF83 disorders, *C. reinhardtii* strains with *SPEF2* and *DNALI1* mutations were isolated and shown to have impaired motility [16][17]. Finally, we've developed an in-house pipeline to track and quantify single-cell motility, facilitating experiments for differentiating healthy and aberrant swimming behavior [18].

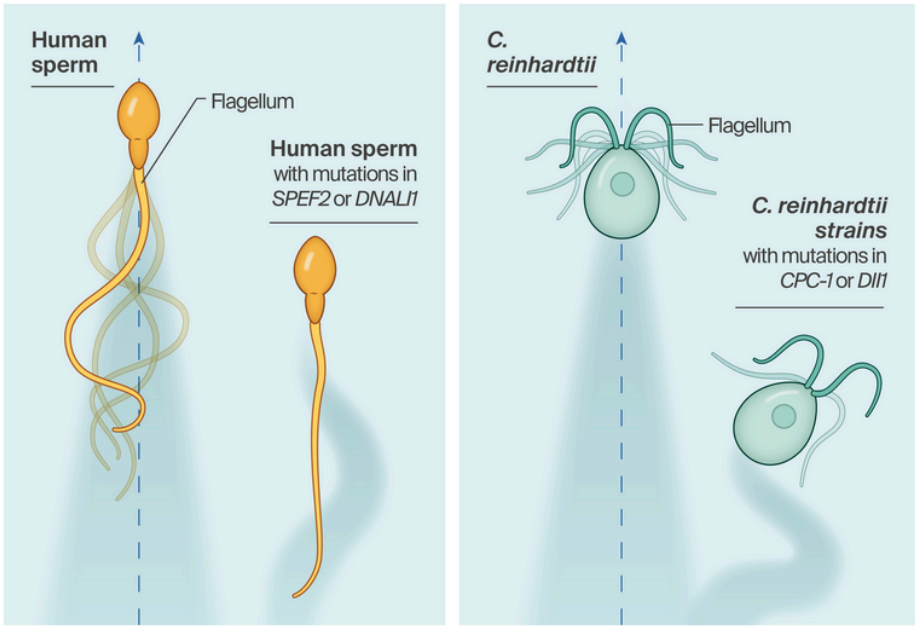

Figure 2. **Graphic of flagellar motility in human sperm and *Chlamydomonas reinhardtii* with SPGF mutations**.

(Left panel) Healthy human sperm showing normal flagellar movement. The flagellum's whip-like motion propels the sperm forward. Human sperm with mutations in *SPEF2* or *DNALI1* exhibit impaired flagellar function, leading to a lack of motility and infertility in patients.

(Right panel) Wild-type *C. reinhardtii* with regular flagellar beating enabling forward motility. *C. reinhardtii* strains with mutations in *CPC-1* or *DII1* (homologs of human genes *SPEF2* and *DNALI1*) show flagellar motion defects. The flagella exhibit uncoordinated or weakened movements, leading to ineffective propulsion and an erratic or reduced swimming pattern.

The *C. reinhardtii* gene *CPC1* (central pair complex 1) is homologous to human *SPEF2* and is disrupted in the mutant *cpc1-1* (CC-3707). These cells have reduced flagellar beat frequencies and disrupted axoneme structures [16][19]. Similarly, the *C. reinhardtii* gene *DII1* (dynein inner arm-interacting 1) is homologous to human *DNALI1*. It's disrupted in the inner dynein arm mutant *ida4* (CC-2670), which has shorter flagella and slower swimming velocity than wild-type cells. Structural and biochemical analysis showed loss of I-projections in the flagellar axoneme [17] and loss of specific dynein subspecies [20]. Based on sequence and structure homology and the nature of the mutations, these *C. reinhardtii* strains may be ideal organisms to model SPGF43 and SPGF83 sperm (Table 1).

A recent, high-throughput screen of ~17,000 compounds on healthy human sperm found 105 compounds that positively affect sperm motility [21]. These results are a

promising step towards treatments for male infertility. However, unknown genetic mutations are often the cause of male infertility, so testing these compounds on human sperm samples with these genetic backgrounds isn't feasible. Because these drugs may influence various mutant sperm differently than wild-type sperm, possibly even reducing motility, the clinical utility of these drugs is unclear. Therefore, we leveraged the structural and functional similarities between *C. reinhardtii* and human sperm, along with our in-house motility assays, to test whether these compounds could restore wild-type motility in mutants with structural defects.

Briefly, we found that drugs affecting human sperm motility could rescue *Chlamydomonas* mutants modeling SPGF, though each drug's effectiveness was mutation-specific. Skip straight to these results or keep reading to understand our methodological approach.

The approach

To model human SPGF disease, we selected motility-impaired *Chlamydomonas reinhardtii* strains with gene mutations known to cause spermatogenic failure in humans. To confirm that we could measure the motility defects, we employed a two-pronged approach: an endpoint assessment of the gross proportion of swimming cells and a quantitative analysis of cell trajectories using time-lapse microscopy. This combination allowed us to evaluate these mutants' overall motility and specific movement characteristics.

We selected a subset of compounds with the most potent positive effects on human sperm motility from a recent screen **[21]** based on their activity and availability (Table 2). Given that many effective drugs influenced metabolism, we also included purified ATP, as ATP availability may modulate metabolism **[22]**. Additionally, because DNALI1 is a component of a dynein complex, we hypothesized that the dynein inhibitor, dynarrestin, could mimic mutant motility in wild-type cells and included this drug in our study. However, we couldn't find any literature describing the impact of this drug on *C. reinhardtii* cells and it’s unlikely to impact flagellar beating since it specifically targets cytoplasmic dynein, rather than axonemal dyneins **[23]**.

To test the ability of these drugs to restore wild-type motility in *C. reinhardtii* mutants, we designed a small-scale chemical screen. Unlike previous efforts, which primarily identified compounds that either decreased motility or affected complex pathways like phototaxis [24][25], our approach aimed to directly quantify the impact of selected compounds on both the quality and quantity of swimming cells.

Read on for the nitty-gritty details on this approach, or skip to the results.

Cell maintenance

After receiving strains from the *Chlamydomonas* Resource Center (Table 1), we streaked cells to individual colonies on TAP media with 1.5% agar. We cultured cells from single colonies in liquid TAP media. Then, we seeded them onto plates of TAP media with 1.5% agar to form a confluent lawn at ambient temperature under constant illumination.

Strain	Description	Disease model
CC-125	Wild-type mt+ [137c]	-
CC-2670	*ida4* mt+	Spermatogenic failure 83
CC-3707	*cpc1-1* mt-	Spermatogenic failure 43

Table 1. ***Chlamydomonas reinhardtii* strains we used in this pub**.
Strain names link to corresponding entries on the *Chlamydomonas* Resource Center website.

Treatment preparation

We selected six compounds to test in our experiments (Table 2). We made 50 mM stocks of Torin2 (Ambeed, Cat # A107433), TAK-063/balipodect (Ambeed, Cat # A579863), linsitinib (Ambeed, Cat # A139562), ibudilast (Ambeed, Cat # A1472713) and dynarrestin (Cayman Chemical, Item # 35527) dissolved in DMSO. We made a 50 mM stock of 99% pure adenosine 5′-triphosphate (ATP) disodium salt hydrate (Sigma-Aldrich, Item # A7699) dissolved in water. We stored all stock solutions at −20 °C, except for ibudilast, which we stored at 4 °C. Based on similar experiments, we diluted stock solutions to 100 µM working concentrations in water before experimentation [24][25]. We added these solutions to cells in TAP

medium at 1:1, resulting in a final concentration of 50 µM. The final DMSO concentration was 0.1% for compounds initially dissolved in DMSO. Accordingly, we used 0.1% DMSO as a negative control, along with a no-DMSO condition.

Drug	MOA	Effect on human sperm curvilinear velocity, %	Effect on *C. reinhardtii* motility	Source	Batch/ lot no.	CAS no.
Torin2	mTOR inhibitor	196	-	Ambeed: A107433	A107433-002	1223001-51-1
TAK-063 (balipodect)	PDE10A inhibitor	145	-	Ambeed: A579863	A579863-001	1238697-26-1
Linsitinib	IGF-1R inhibitor	191	-	Ambeed: A139562	A139562-002	867160-71-2
Ibudilast	PDE inhibitor	167	Increased phototaxis	Ambeed: A1472713	A1472713-QA3	17877835
Dynarrestin	Dynein inhibitor	-	-	Cayman Chemical: 35527	0641251-6	2222768-84-3
ATP disodium salt hydrate	Energy	-	-	Sigma-Aldrich: A7699	SLCJ5924	34369-07-08

Table 2. **Treatments in this study**.

Abbreviations: MOA = mechanism of action; mTOR = molecular target of rapamycin; PDE = phosphodiesterase; IGF-1R = insulin-like growth factor 1 receptor; ATP = adenosine 5′-triphosphate; DMSO = dimethylsulfoxide; no. = number; TAK = Takeda Pharmaceutical Company Limited. Effects on human sperm were reported by Gruber et al. 2022 **[21]**.

V-bottom motility assay

To assess the fraction of motile cells, we conducted imaging experiments with cells growing in v-bottom plates where the non-motile cells should collect in the center of the well. We used a sterile loop to collect cells from TAP media + 1.5% agar plates and resuspended the cells in liquid TAP media. We then passed the cells through a 40 µm pore nylon mesh cell strainer (Falcon, Product 352340) to remove cell clumps. Next, we centrifuged the cells at 2,500 × g for 5 min and resuspended the pellets in fresh TAP media. We measured each culture's optical density at 730 nm using a SpectraMax iD3 plate reader (Molecular Devices). We

then diluted cultures with TAP medium to normalize the concentrations across samples.

For the analyses presented in Figure 3, we allowed the diluted cultures to adapt to their liquid environment overnight. We seeded 100 µL of dense cultures the next day into a 384-well v-bottom plate (Greiner Bio-One, Product 781280). We immediately placed the plate on a "phenotype-o-mat" enclosed in a dark box to block outside light and imaged at one frame per minute for 96 frames [26]. We used the final frame acquired for analysis.

For the analyses presented in Figure 5, we seeded 100 µL of cells into a 96-well v-bottom plate (Corning, product 3896). We added 100 µL of the indicated treatment, resulting in a final volume of 200 µL and a concentration of 50 µM. We mixed the cells and treatments by pipetting up and down with a multi-channel pipette. Next, we immediately placed the plate on a phenotype-o-mat [26] under a dark box to block outside light and imaged at one frame per hour over four days to allow the diluted cell cultures adequate time to adapt and grow.

For all experiments, we exposed the samples to constant illumination from the phenotype-o-mat for the duration of the experiment. We used a Blackfly S USB camera to acquire these images. We turned on the LED ring (featuring 460 nm, 535 nm, 590 nm, and 670 nm wavelength LEDs) between image acquisitions to act as a grow light.

Single-cell tracking sample preparation

To measure statistics derived from the motility of single cells, we grew cultures for two days in liquid TAP media on a rotating drum under a 12:12 light-dark cycle. On the day of the experiment, we measured the optical density of each culture at 690 nm (OD_{690}) using a SpectraMax iD3 plate reader (Molecular Devices). We then diluted the cultures to the same concentration (~0.1) based on OD_{690} measurements.

We dispensed 15 µL of the diluted cultures into the wells of a glass-bottom, 384-well plate (Cellvis, Product #P384-1.5H-N). We added 15 µL of the appropriate treatment to each well from a 2× stock, resulting in a final volume of 30 µL at the

desired concentration (1×). We mixed each well by gently pipetting up and down. We let the plate sit in the dark for approximately 2.5 hours before imaging.

We designed the plate layout to include three *C. reinhardtii* strains and six compounds at 50 μM concentrations. We arranged the strains in consecutive row pairs, with duplicate wells for each condition, starting with wild type, then *ida4*, and finally *cpc1-1*. The top six rows contained 12.5 μM drug, 0.0025% DMSO, or water. We repeated this pattern for the next six rows that contained 50 μM drug, 0.01% DMSO, or water. Each column contained a specific treatment, from left to right: Torin2, TAK-063, linsitinib, ibudilast, dynarrestin, ATP, DMSO, and water. For simplicity, we only included 50 μM treatments in our analysis, but the raw imaging data for all treatments are available on the BioImage Archive.

Microscopy

We employed the same image acquisition procedure used in [18]. Briefly, we imaged samples in glass-bottom microtiter plates using a 10× 0.45 NA air objective (Nikon) mounted on an inverted Nikon Ti2-E confocal microscope fitted with an ORCA-Fusion BT digital sCMOS camera (Hamamatsu) and a LIDA Light Engine (Lumencor) for illumination controlled with NIS-Elements software (v5.42.03). We recorded a 20 s time-lapse of each well within the microtiter plate using brightfield microscopy at 20 frames per second (50 ms exposure). We set the light intensity to maximize the dynamic range of the acquisition system and only used red light to avoid phototactic responses caused by broad-spectrum white light. We used the NIS-Elements JOBS module to move between the center of each well automatically.

Since we were conducting high-throughput, high-resolution data acquisition across many live samples with many conditions, cells at the beginning of the plate (imaged first) spent less time in the drug before imaging than cells at the end of the plate (imaged last). We began imaging from the top left well (A1) to address this and progressed along each row. At the end of each row, we began imaging at the beginning of the subsequent row (e.g., well B1 after completing row A). Because we organized strains in pairs of rows, this sampling approach interleaved species samples to provide more similar timing for drug exposure duration across strains rather than simply imaging each strain in succession. It took roughly 40 minutes to acquire the 96 time-lapse images included in our analysis.

Image analysis

We analyzed image data capturing cell motility in v-bottom wells by taking line scan intensity measurements across the wells. We used Fiji (v2.14.0/1.54f) to manually straighten and crop the raw images to include only the wells of interest. Next, we used a Python script to identify the center of each well and take horizontal intensity line scans (40 pixels long and 10 pixels wide) across the center of each well. To ensure accurate comparison across wells, we realigned the intensity profiles based on the position of the cell pellet, which we identified as the lowest intensity value in the central 20 pixels of the scan. We verified the correct positioning of the line scans by having the script save a copy of the raw image with the line scan positions superimposed. We performed statistical analysis with Python (v3.12) using SciPy (v1.14.1) **[27]**, statsmodels (v0.14.3) **[28]**, and scikit-posthocs (v0.10.0) **[29]**. ChatGPT (GPT-4 and GPT-4o) assisted in scripting and commenting on this code.

We analyzed the time-lapse microscopy data capturing single-cell motility using the image processing pipeline described in **[18]**. First, we segmented cells by thresholding the mean background-subtracted time-lapse data, resulting in binarized videos. Next, we tracked cells in binarized time-lapse videos using btrack (v0.6.5) **[30]** with the default configuration files. The output from btrack is a CSV file containing the measured (x, y) coordinates of each cell's trajectory at every frame the cell was tracked. We calculated summary motility metrics, such as the total distance, mean curvilinear velocity, and confinement ratio, from each cell's trajectory using the `compute_motility_metrics.py` script in our GitHub repo. We computed Kernel density estimates of the distributions in Scipy (v1.14.1) based on the implementation described in **[31]** with default smoothing kernels. We performed principal component analysis (PCA) using scikit-learn (v1.4.2) **[32]**.

Writing and coding

We used ChatGPT (GPT-4, GPT-4o, o1-preview), Claude (3.5 Sonnet), and Grammarly (1.92.0.1) to suggest wording ideas, to streamline or clarify content, and to reformat text to our style guide. We then edited the AI-generated text. We used ChatGPT (GPT-4 and GPT-4o) and Claude (3.5 Sonnet) to help write, clean up, and comment on our code.

The results

To identify potential treatments for SPGF43 and SPGF83, genetic forms of male infertility that impair sperm motility, we set out to test whether compounds known to enhance human sperm motility could restore normal swimming in *Chlamydomonas reinhardtii* strains with mutations in the corresponding genes.

Chlamydomonas reinhardtii mutants modeling SPGF have motility defects

Previous analyses found that the two *C. reinhardtii* mutants we used in this study have motility defects [16][17]. To validate these results in-house, we used a simple approach of seeding v-bottom well plates with wild-type and mutant *C. reinhardtii* strains to perform a "sink-or-swim" assay, as schematized in Figure 3, A. In this assay, the non-motile cells collect over time at the bottom of the well, while the healthy swimmers will remain in suspension. We used a "phenotype-o-mat," a customizable DIY plate reader [26][33], to image the accumulation of non-motile cells at the bottom of the wells and collected line scan intensity measurements to quantify motility differences (Figure 3, A). Consistent with having the expected motility defects, both *ida4* and *cpc1-1* cells quickly accumulated at the bottom of the wells, while the wild-type cells remained in suspension for the duration of the experiment (Figure 3, B). To estimate the fraction of non-motile cells (pellet-to-periphery intensity ratio [P2P Ratio]), we divided the minimal intensity value by the average intensity of the peripheral tail (defined as the range of pixels between positions 33 and 37 of the 40-pixel line scan) for each line scan. This analysis revealed significantly more non-motile *ida4* cells and *cpc1-1* cells compared to wild-type (WT) cells (P2P Ratio of *ida4* vs. WT, Kruskal–Wallis test with Dunn's post-hoc test, p = 4e–4; P2P Ratio of *cpc1-1* vs. WT, Kruskal–Wallis test with Dunn's post-hoc test, p = 8.7e–14). Further, there were significantly more non-motile *cpc1-1* cells compared to *ida4* cells (Kruskal–Wallis test with Dunn's post-hoc test, p = 4.3e–04), indicating that the *cpc1-1* mutant modeling SPGF43 has a more severe motility defect (Figure 3, C).

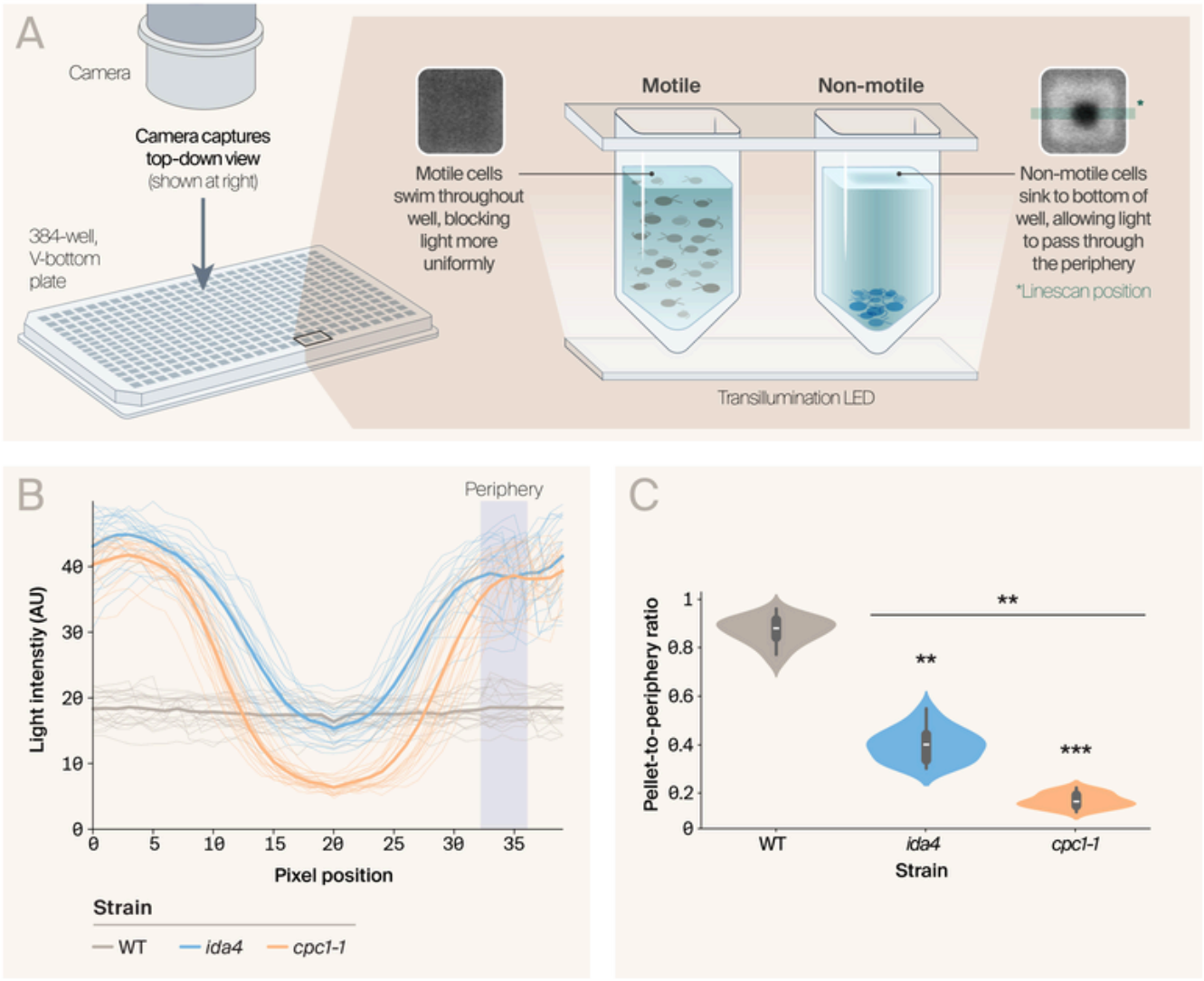

Figure 3. ***Chlamydomonas reinhardtii* mutants modeling SPGF have reduced overall motility**.

(A) Graphic depicting our sink-or-swim assay in which a 384-well v-bottom plate is illuminated from below by LEDs while a camera records from above. Motile cells stay in suspension, scattering light uniformly and reducing the amount of light reaching the camera. Non-motile cells sink to the bottom, forming a dense pellet in the center that blocks light, creating a dark spot surrounded by a bright edge where light passes unobstructed. This setup allows for differentiation between swimming and sinking cells based on their effect on light transmission. We show representative images of dense *Chlamydomonas reinhardtii* cultures in a conical-bottom plate after 1.72 hours on the phenotype-o-mat.

(B) Intensity measurements from line scans show the average intensity across each well with a 10-pixel-wide line scan. Thin lines represent individual scans, while bold lines show the average intensity of line scans across 22 individual wells for the indicated strain (n = 22). The shaded area represents the peripheral pixel intensities we averaged to calculate pellet-to-periphery intensity ratios. We normalized intensity values to the average intensity per well to correct for variation in culture density.

(C) Violin plots of the pellet-to-periphery intensity ratios. We performed pairwise comparisons of strain motility using the Kruskal–Wallis test with Dunn's post-hoc test (H-statistic: 57.7910; p-value: 0.0000). **: $p < 0.01$, ***: $p < 0.001$. Floating asterisks represent a comparison to WT. A line under the asterisk indicates a comparison of the conditions underneath the line.

Many mechanisms could cause the differences in motility we found in this bulk assay. To better understand why these mutants have reduced motility, we turned to a second assay — a quantitative, single-cell tracking pipeline called "SwimTracker" that we recently developed [18]. To ensure we were imaging live swimming cells, we selected a z-plane approximately halfway through the volume of liquid and acquired time-lapse microscopy data as described in "Microscopy."

Our analysis pipeline tracks individual cells within time-lapse microscopy data and computes several motility metrics to quantify the nature of each cell's trajectory. The motility metrics assessed here include:

- Max sprint length: The maximum distance traveled in a short (0.25 s) interval
- Confinement ratio: The net (start-to-end) distance ratio to the total distance
- Mean curvilinear speed: The average speed of a cell along its curved trajectory
- Mean linear speed: The average speed of a cell along a straight path between its start and end point
- Mean angular speed: The average rate of angular change
- Pivot rate: The ratio of the number of directional changes to the total distance

(For a visual representation of these metrics and how they're calculated, refer to "A high-throughput imaging approach to track and quantify single-cell swimming," Figure 4) [18].

We show typical cell trajectories from wild-type and mutant strains in Figure 4, A. Wild-type swimming is generally characterized by faster, straighter trajectories, while mutant swimming tends to be slower and more meandering. This behavior is reflected in motility metrics like the max sprint length, which was 45% and 30% lower for *ida4* and *cpc1-1* mutants, respectively, and the mean linear speed, which was 44% and 56% lower for *ida4* and *cpc1-1* mutants, respectively (Mann–Whitney U, $p < 0.001$) (Supplemental Figure 1).

Since these motility measurements are interrelated, we used principal component analysis (PCA) to identify independent patterns in our data. PCA transforms our correlated motility metrics into separate components representing distinct aspects of swimming behavior while allowing direct comparisons between wild-type and

mutant cells. We built our models using normalized motility metrics from wild-type and mutant strains in control conditions (water and 0.1% DMSO). A model was constructed for each mutant to compare each strain to wild-type individually. The analysis included six rate-based measurements: mean curvilinear speed, linear speed, angular speed, max sprint length, confinement ratio, and pivot rate. We used only rate-based metrics due to the variance in trajectory durations (10–20 s).

By examining how different motility metrics contributed to each principal component, we could better understand what aspects of swimming behavior they represent. The first principal component (PC1) primarily captures confinement ratio, mean linear speed, and pivot rate, while the second principal component (PC2) represents max sprint length, mean curvilinear speed, and mean linear speed (Figure 4, B–C). We found that the motility behaviors of both *ida4* and *cpc1-1* were significantly different from wild type, consistent with the previously reported motility defects [17][19]. Specifically, although we couldn't distinguish *ida4* from wild-type cells in PC1 (Mann–Whitney *U* test, $p = 0.35$), there was a substantial shift in PC2 (Mann–Whitney *U* test, $p = 4.4e{-}11$) (Figure 4, B). Consistent with our v-bottom assay, *cpc1-1* motility defects were much more pronounced. We could clearly distinguish these mutants from wild-type strains in PC1 (Mann–Whitney *U* test, $p = 3.4e{-}13$) and PC2 (Mann–Whitney *U* test, $p = 0.0058$) (Figure 4, C). Because these strains have motility defects consistent with low sperm motility, we next asked if we could treat the mutants with drugs to recover the wild-type phenotype.

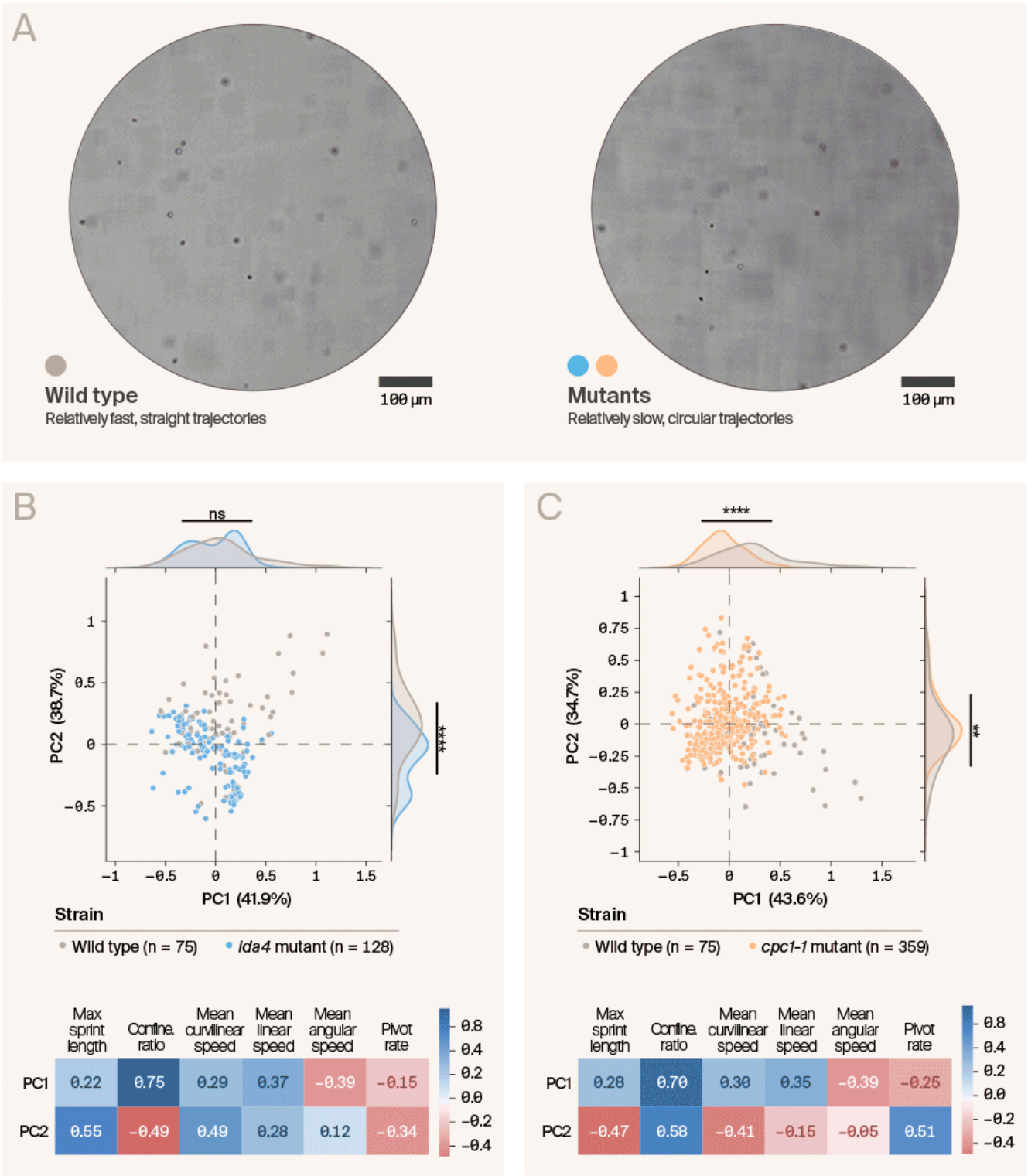

Figure 4. ***Chlamydomonas reinhardtii* strains modeling SPGF have distinct motility behaviors.**

(A) Videos of tracked wild-type cells (left) with animated trails illustrating faster and straighter trajectories relative to *cpc1-1* mutant cells (right), which tend to meander slowly. Videos are real-time, at 20 fps.

(B, C) PCA of *C. reinhardtii* motility for wild-type and two mutant strains showing the distribution of wild-type vs. *ida4* cells (B) and wild-type vs. *cpc1-1* cells (C) in the fitted PC space. The kernel density estimate of each principal component is plotted along the margin. **: $p < 0.01$; ****: $p < 0.0001$; ns: no statistical significance. Heatmaps indicate the PCA weights. PC1 explains 41.9% (B) or 43.6% (C) of the variance; PC2 explains 38.7% (B) or 34.7% (C) of the variance.

Drug treatments rescue *Chlamydomonas reinhardtii* motility in mutants

Having demonstrated that, similar to their human homologs, loss-of-function mutations in *CPC1* and *DII1* lead to motility defects, we next sought to identify molecules that could recover these defects. We focused on molecules previously shown to positively influence wild-type human sperm motility. If we can demonstrate that compounds affecting human sperm motility similarly impact *C. reinhardtii* motility, this would further validate *C. reinhardtii* as a model for studying sperm motility. Moreover, if these molecules can restore wild-type motility, they may offer potential therapeutic options for certain types of SPGF and serve as valuable tools for investigating the biology of these mutants.

We selected a limited panel of small molecules reported to increase the motility of healthy human sperm [17]. Briefly, we selected the mammalian target of rapamycin (mTOR) inhibitor Torin2, the phosphodiesterase (PDE) inhibitor ibudilast, the phosphodiesterase 10A (PDE10A) inhibitor TAK-063/balipodect, and the insulin-like growth factor 1 receptor (IGF-1R) inhibitor linsitinib. We included the dynein inhibitor dynarrestin, expecting to recapitulate *ida4* defects in wild-type cells since *ida4* mutants have impaired dynein; however, this inhibitor specifically targets cytoplasmic dynein rather than axonemal dynein, reducing its likelihood to impact flagellar motility [23]. We also included pure ATP since many of the compounds that increase healthy sperm motility impact metabolism. We used water or 0.1% DMSO as controls for the solvents (Table 2).

To determine if these compounds impact the swimming behavior of mutant strains, we performed the motility assays described above under eight individual conditions (six drug treatments and two controls). First, we repeated the v-bottom sink-or-swim assay. Although we selected four of these drugs due to reports of increased curvilinear velocity of human sperm [21], we found that the IGF-1R inhibitor linsitinib significantly reduced the pellet-to-periphery intensity ratio of wild-type cells when compared to control (Figure 5, left; Table 3). Similarly, the motility defect of *ida4* cells worsened when treated with linsitinib and ibudilast; however, Torin2 did significantly recover motility in these cells (Figure 5, middle; Table 3).

In contrast, none of the treatments worsened *cpc1-1*'s impaired motility phenotype. In fact, we observed an improvement in *cpc1-1* motility when treated with ibudilast, linsitinib, or Torin2 (Figure 5, right; Table 3). Noticeably, across all strains, Torin2 treatment reduced the accumulation of cells in the bottom of wells. However, the transmitted light intensity was consistently high, suggesting that while Torin2 may rescue motility, it actively reduces cell growth (Figure 5, A, blue lines). This is consistent with Torin2's ability to reduce the growth of human cancer cells or parasitic *Plasmodium* species **[34][35][36]** and the ability of different mTOR inhibitors to reduce *Chlamydomonas* growth **[37]**.

These strain-specific drug responses reveal important insights about SPGF treatment. Despite having similar structural defects and swimming phenotypes, our *C. reinhardtii* strains modeling different SPGF disorders showed distinct and sometimes opposite responses to the same compounds. For example, while linsitinib improved *cpc1-1* motility, it worsened *ida4* swimming — highlighting that genetically distinct forms of SPGF may require different therapeutic approaches. This specificity in drug response suggests that effective SPGF treatments might need to be tailored to specific genetic mutations rather than treating all motility defects the same way.

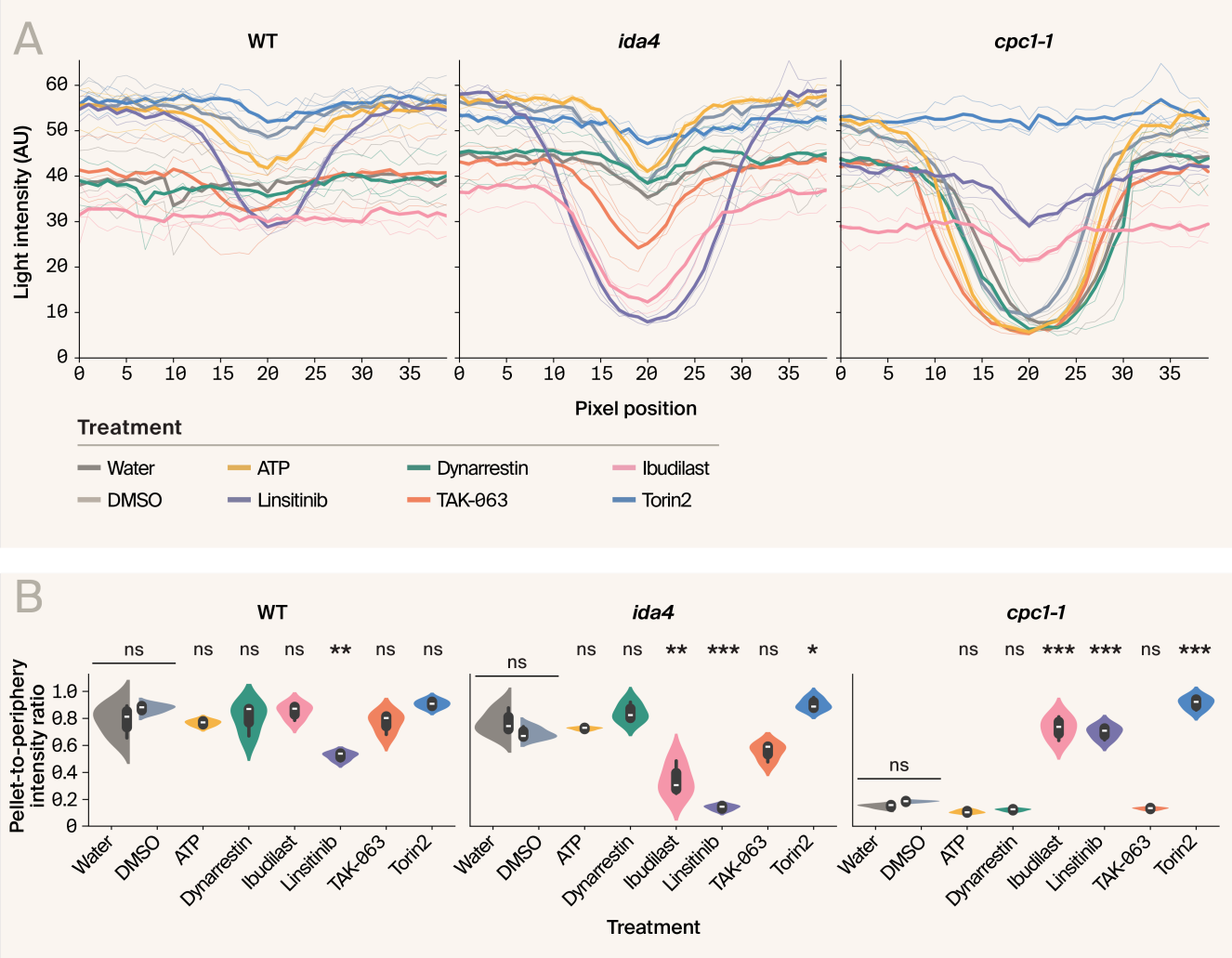

Figure 5. **Effects of drugs on *Chlamydomonas reinhardtii* WT and mutant cell motility**.

(A) Intensity measurements from line scans show the average intensity across each well with a 10-pixel-wide line scan. Thin lines represent individual scans, while bold lines show the average intensity for the indicated strain. We performed each treatment in triplicate (*n* = 3). We acquired the data after 95 hours of treatment. We didn't normalize this dataset to highlight drug-induced growth effects.

(B) Violin plots of the pellet-to-periphery intensity ratios. We performed ANOVA with Tukey's post-hoc test to compare the fraction of motile to non-motile cells across treatments, independently for each strain. Individual pairwise comparisons can be found in our GitHub repo. ANOVA results: WT, F(7,16) = [12.3], p = 2.2e–05; *ida4*, F(7,16) = [41.9], p = 4.1e–09; *cpc1-1*, F(7,16) = [99.0], p = 5.7e–12. ****: $p < 0.0001$; ***: $p < 0.001$; **: $p < 0.01$; *: $p < 0.05$; and ns denotes no statistical significance. Floating asterisks represent a comparison to the appropriate control. A line under the asterisk indicates a comparison of the conditions underneath the line.

Strain	ATP vs. water	Dynarrestin vs. DMSO	Ibudilast vs. DMSO	Linsitinib vs. DMSO	TAK-063 vs. DMSO	Torin2 vs. DMSO	DMSO vs. water
WT	0.9999	0.9171	0.9999	0.0004	0.6432	0.9989	0.8012
ida4	0.9866	0.1905	0.0003	0.0	0.3066	0.0267	0.8096
cpc1-1	0.9201	0.6062	0.0	0.0	0.7646	0.0	0.9615

Table 3. ***P*-values from pairwise comparisons using ANOVA and Tukey's test assessing the effects of drugs on the pellet-to-periphery ratio**.

Treatments include adenosine 5′-triphosphate (ATP), dynarrestin, ibudilast, linsitinib, TAK-063, and Torin2. We considered p-values < 0.05 statistically significant.

Our finding that many of these drugs influence the overall fraction of motile cells motivated an investigation into their impact on various individual dimensions of cellular motility. We examined the swimming trajectories of these *C. reinhardtii* strains with each of the drug treatments described above using our single-cell tracking assay. As before, we imaged at a z-plane above the coverslip to capture motile cells. Our analysis determines whether motility differs between the wild type and the treated mutant. If we observe no significant difference, it usually indicates that the drug restores wild-type motility in that dimension. However, since *ida4* and wild-type motility were indistinguishable in PC1 (Figure 4, C) we're unable to claim any drugs rescued PC1 behavior in these mutants. Nevertheless, ibudilast and Torin2 clearly impacted *ida4* PC1 motility, shifting the density away from the mutant and wild type cells, with ibudilast negatively shifting PC1 and Torin2 increasing PC1 (Figure 6, B; Table 4).

When we treated *ida4* cells with ATP, dynarrestin, ibudilast, linsitinib, or TAK-063, we observed a recovery of wild-type motility behaviors captured in PC2. However, Torin2 couldn't rescue wild-type PC2 attributes in *ida4* cells (Figure 6, B and E; Table 4). Further, *cpc1-1*, which has a more obvious motility defect (Figure 3 and Figure 4), had a clear recovery in wild-type PC1 and PC2 motility behaviors when we treated the cells with TAK-063 or Torin2. ATP, dynarrestin, and linsitinib recovered wild-type behaviors captured in PC1 but not PC2. Treatment with ibudilast didn't appear to recover wild-type swimming behaviors captured in either PC1 or PC2 (Figure 6, C and F; Table 4).

We observed some interesting disparities when comparing these single-cell tracking results to the bulk motility assay. For instance, Torin2 improved bulk motility in both mutants but showed contrasting effects in the detailed motion analysis, worsening both PC1 and PC2 behaviors in *ida4* while successfully restoring wild-type levels in *cpc1-1*. Similarly, compounds like ATP and dynarrestin showed different impacts between assays—in single-cell tracking they recovered wild-type PC1 behavior in *cpc1-1* but failed to restore PC2, while showing minimal effects in the bulk assay. These discrepancies between assays could be explained by their different experimental setups — the bulk assay captures the entire population's swimming behavior, including the proportion of motile to non-motile cells, while the single-cell tracking specifically examines the movement patterns of actively swimming cells. Rather than individual behaviors explaining a cell's ability to stay in suspension, this combination of approaches provides complementary insights into how these compounds affect different aspects of cellular motility.

While these data strongly suggest *C. reinhardtii* is an excellent organism to study spermatogenic failure, we were surprised that most of the compounds tested didn't affect the swimming behavior of motile wild-type *C. reinhardtii* cells (Figure 6, A and D; Table 4). The lack of a positive impact of these drugs on wild-type *C. reinhardtii* was unexpected since we'd selected them for their reported positive effect on the curvilinear velocity of healthy human sperm **[21]**.

To better understand how our data compare to that of sperm in the literature, we specifically checked the mean curvilinear speed of wild-type *C. reinhardtii* under each of these conditions. We were again surprised that most compounds didn't affect wild-type *C. reinhardtii* speed (Mann–Whitney *U* test, control vs. dynarrestin: $p = 0.92$; control vs. linsitinib: $p = 0.062$; control vs. TAK-063: $p = 0.23$; control vs. Torin2: $p = 0.080$). Only ATP was able to increase the speed of wild-type *C. reinhardtii* (Mann–Whitney *U* test, control vs. ATP: $p = 0.026$), consistent with the literature on this species **[38][39][40]** (Supplemental Figure 2).

The limited impact of these compounds on wild-type *C. reinhardtii* motility, despite their known effects on human sperm, highlights important species differences in motility regulation. While both systems use similar flagellar machinery, the cellular pathways that modulate swimming behavior may differ between species. For instance, the IGF-1R pathway targeted by linsitinib might play a more central

role in human sperm motility than in *C. reinhardtii*. Nevertheless, the fact that these compounds can rescue motility in our mutant strains suggests that flagellar dysfunction might make cells more responsive to metabolic and signaling perturbations across species. These results support *C. reinhardtii* as a model specifically for studying motility defects, even if baseline motility regulation differs between species.

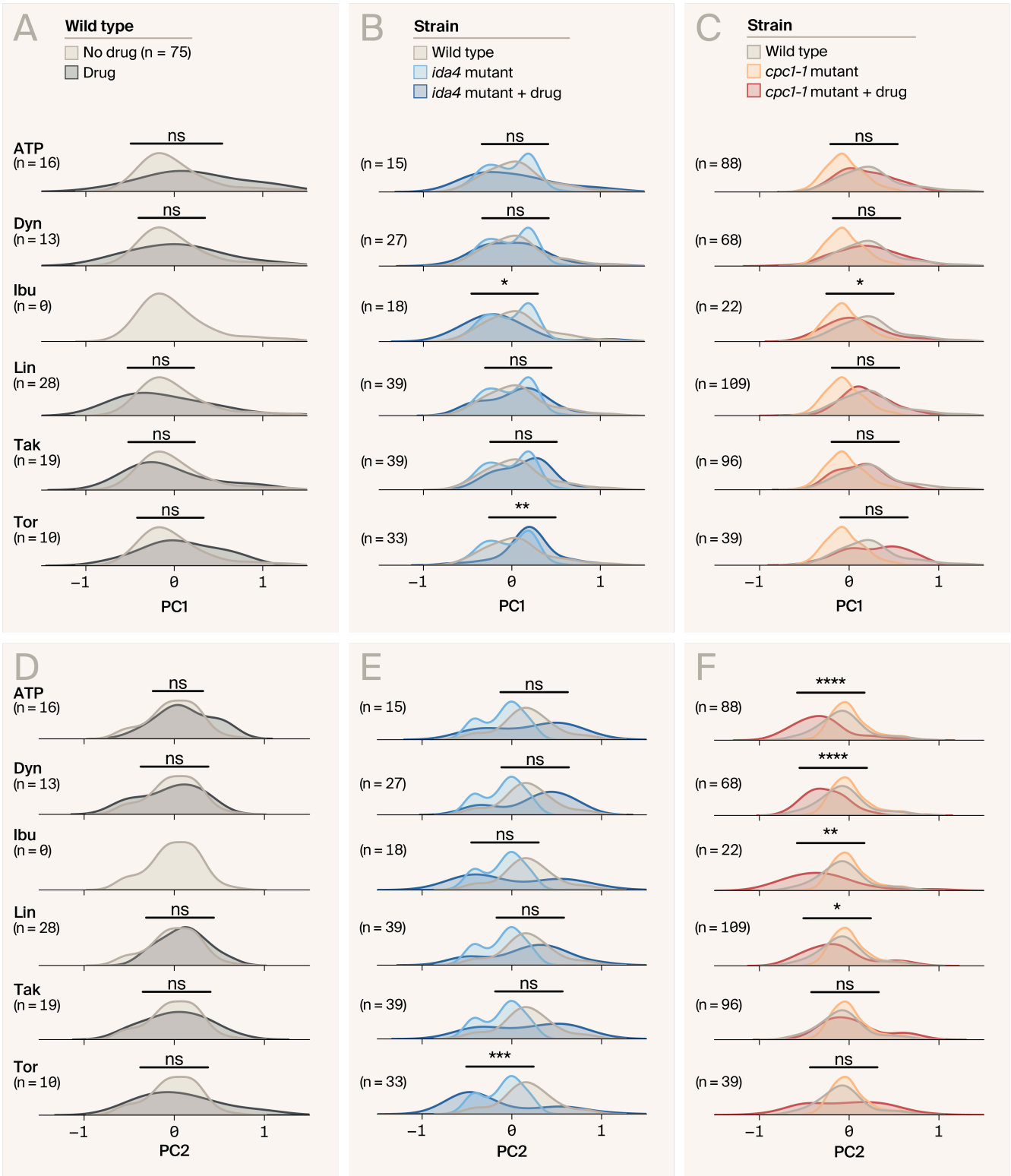

Figure 6. **Effects of drugs on cell motility behavior**.

Kernel density estimates of the first (A–C) and second (D–F) principal components showing the response of wild type (A, D), *ida4* (B, E), *cpc1-1* (C, F) strains to each drug in the small molecule panel. We applied each drug at a 50 μM concentration. ****: $p < 0.0001$; ***: $p < 0.001$; **: $p < 0.01$; *: $p < 0.05$; and ns denotes no statistical significance. We didn't test ibudilast in wild-type cells because of limited reagents on the day of experimentation.

	ATP		Dynarrestin		Ibudilast		Linsitinib		TAK-063		T
	PC1	PC2	PC1	PC2	PC1	PC2	PC1	PC2	PC1	PC2	P
WT vs. WT + drug	0.07	0.21	0.72	0.93	-	-	0.18	0.15	0.39	0.73	
WT vs. *ida4* + drug	0.48	0.54	0.60	0.053	0.014	0.3	0.52	0.58	0.068	0.72	
WT vs. *cpc1-1* + drug	0.5	5.8e–8	0.72	2.7e–5	0.035	0.0012	0.65	0.023	0.067	0.064	

Table 4. ***P*-values from pairwise comparisons using the Mann–Whitney *U* test, assessing the effects of various drugs on cell trajectories**.

Treatments include adenosine 5′-triphosphate (ATP), dynarrestin (Dyn), ibudilast (Ibu), linsitinib (Lin), TAK-063 (TAK), and Torin2 (Tor). We considered p-values < 0.05 to be statistically significant.

We took a two-pronged approach to measure cell motility, but the results often varied between our two assays (summarized in Table 5). For example, TAK-063 restored motility in both *ida4* and *cpc1-1*, but we only observed this effect in the cell trajectory assay. Similarly, ibudilast recovered wild-type motility in *cpc1-1* in the v-bottom assay, but only restored motility in *ida4* with the cell trajectory assay. On the other hand, Torin2 restored motility in *cpc1-1* with both assays, but didn't restore single-cell swimming behaviors in *ida4*, suggesting it may target a pathway specifically disrupted in *cpc1-1* cells.

Together, these results highlight the complexity of how different small molecules interact with specific pathways, even in similar mutants that share a similar phenotype. The distinct effects of each drug underscore the diversity of molecular targets involved in motility. Additionally, the unique outcomes of each assay reflect the variety of biological mechanisms contributing to flagellar motility. Future studies could focus on identifying which metrics of sperm motility are most crucial to address when treating patients with specific SPGF disorders. Beyond discovering potential new therapies for SPGF disorders, these findings offer valuable insights into the biological differences between these mutant strains and deepen our understanding of the complexities of flagellar motility.

	V-bottom bulk assay		Single-cell trajectory assay			
	Overall motility		PC1		PC2	
Drug	*ida4*	*cpc1-1*	*ida4*	*cpc1-1*	*ida4*	*cpc1-1*
ATP	=	=	=			
Dynarrestin	=	=	=			
Ibudilast				=		
Linsitinib			=			
TAK-063	=	=	=			
Torin2						

Table 5. **Summary of treatment effects**.
= decreased; **=** = no change; = increased; = recovered

Key takeaways

Although we selected compounds already reported to increase sperm motility, our results indicate that we'd have identified each of these compounds as potential therapeutics had we done a larger, non-targeted screen of small-molecule compounds. They all showed a positive effect on motility in at least one assay or strain.

- We successfully rescued various aspects of motility in *C. reinhardtii* flagellar mutants using the compounds Torin2, ibudilast, linsitinib, and TAK-063, demonstrating the potential of these molecules to restore motility in genetic models of spermatogenic failure (Table 4).
- Our findings show that potentially therapeutic responses vary substantially between different mutants, even when they share a similar phenotype. This underscores the complexity of genetic diseases and the importance of developing mutation-specific treatments for effective therapy.
- We found evidence that genetically and experimentally tractable organisms like *Chlamydomonas reinhardtii* are good candidates for modeling human diseases such as SPGF, enabling the discovery of potential therapeutic interventions.
- We've developed and validated tools that are easily adaptable for high-throughput motility assays across various organisms and research questions, facilitating broader applications in genetic and drug discovery studies.

Next steps

This work lays the groundwork for discovering novel therapeutics for various diseases beyond SPGF. Flagellar motility is crucial in various cellular functions related to human health, with the OMIM database listing over 270 individual ciliopathies. Leveraging flagellar motility in an organism with a robust genetic toolkit and a collection of over 60,000 accessible mutant strains presents a unique opportunity to quickly and inexpensively screen molecules that could serve as therapeutics for these conditions.

It's important to note that the small molecules used in these experiments aren't FDA-approved for human use. However, this approach could be scaled up to screen FDA-approved compounds in high throughput to identify potential treatments for various diseases.

Our analysis also identified the picoplankton species *Micromonas commoda* as a model to study SGPF43 (Figure 1). Although *M. commoda* mutants aren't as widely available as *C. reinhardtii*, genetic tools do exist [41], and the swimming behavior of these algae may be more similar to human sperm since they have a single flagellum [42][43], providing another promising path to study this disease.

While we don't plan to continue pursuing therapeutics for SPGF, we strongly encourage others in the scientific community to build upon this foundation.

Contributors (A–Z)

- **Audrey Bell**: Visualization
- **Tara Essock-Burns**: Critical Feedback, Formal Analysis, Investigation, Supervision
- **Megan L. Hochstrasser**: Editing
- **Ryan Lane**: Formal Analysis, Software
- **Cameron Dale MacQuarrie**: Conceptualization, Formal Analysis, Investigation, Visualization, Writing
- **David G. Mets**: Software, Supervision

References

1. Inaba K. (2011). Sperm flagella: comparative and phylogenetic perspectives of protein components. https://doi.org/10.1093/molehr/gar034
2. Bell A, Essock-Burns T, Lane R, Hochstrasser M, MacQuarrie CD, Mets D. (None). Data underlying the pub "Rescuing Chlamydomonas motility in mutants modeling spermatogenic failure". https://doi.org/10.6019/s-biad1470
3. Mitchell DR, Sale WS. (1999). Characterization of a Chlamydomonas Insertional Mutant that Disrupts Flagellar Central Pair Microtubule-associated Structures. https://doi.org/10.1083/jcb.144.2.293
4. https://www.who.int/publications/i/item/978920068315
5. Kamiya R, Kurimoto E, Muto E. (1991). Two types of Chlamydomonas flagellar mutants missing different components of inner-arm dynein.. https://doi.org/10.1083/jcb.112.3.441
6. Visser L, Repping S. (2010). Unravelling the genetics of spermatogenic failure. https://doi.org/10.1530/rep-09-0229
7. Essock-Burns T, Lane R, Mets DG. (2024). A high-throughput imaging approach to track and quantify single-cell swimming. https://doi.org/10.57844/arcadia-2d61-fb05
8. Grimes DA, Lopez LM. (2007). “Oligozoospermia,” “azoospermia,” and other semen-analysis terminology: the need for better science. https://doi.org/10.1016/j.fertnstert.2007.04.013
9. Zhang H, Mitchell DR. (2004). Cpc1, aChlamydomonascentral pair protein with an adenylate kinase domain. https://doi.org/10.1242/jcs.01297
10. Celebi FM, Chou S, McGeever E, Patton AH, York R. (2023). NovelTree: Highly parallelized phylogenomic inference. https://doi.org/10.57844/arcadia-z08x-v798
11. Kagami O, Kamiya R. (1992). Translocation and rotation of microtubules caused by multiple species of Chlamydomonas inner-arm dynein. https://doi.org/10.1242/jcs.103.3.653
12. Avasthi P, McGeever E, Patton AH, York R. (2024). Leveraging evolution to identify novel organismal models of human biology. https://doi.org/10.57844/arcadia-33b4-4dc5
13. Gruber FS, Johnston ZC, Norcross NR, Georgiou I, Wilson C, Read KD, Gilbert IH, Swedlow JR, Martins da Silva S, Barratt CLR. (2022). Compounds

enhancing human sperm motility identified using a high-throughput phenotypic screening platform. https://doi.org/10.1093/humrep/deac007

14. Liu C, Lv M, He X, Zhu Y, Amiri-Yekta A, Li W, Wu H, Kherraf Z-E, Liu W, Zhang J, Tan Q, Tang S, Zhu Y-J, Zhong Y, Li C, Tian S, Zhang Z, Jin L, Ray P, Zhang F, Cao Y. (2019). Homozygous mutations in SPEF2 induce multiple morphological abnormalities of the sperm flagella and male infertility. https://doi.org/10.1136/jmedgenet-2019-106011
15. Bonora M, Patergnani S, Rimessi A, De Marchi E, Suski JM, Bononi A, Giorgi C, Marchi S, Missiroli S, Poletti F, Wieckowski MR, Pinton P. (2012). ATP synthesis and storage. https://doi.org/10.1007/s11302-012-9305-8
16. Liu W, Sha Y, Li Y, Mei L, Lin S, Huang X, Lu J, Ding L, Kong S, Lu Z. (2019). Loss-of-function mutations in SPEF2 cause multiple morphological abnormalities of the sperm flagella (MMAF). https://doi.org/10.1136/jmedgenet-2018-105952
17. Höing S, Yeh T-Y, Baumann M, Martinez NE, Habenberger P, Kremer L, Drexler HC, Küchler P, Reinhardt P, Choidas A, Zischinsky M-L, Zischinsky G, Nandini S, Ledray AP, Ketcham SA, Reinhardt L, Abo-Rady M, Glatza M, King SJ, Nussbaumer P, Ziegler S, Klebl B, Schroer TA, Schöler HR, Waldmann H, Sterneckert J. (2018). Dynarrestin, a Novel Inhibitor of Cytoplasmic Dynein. https://doi.org/10.1016/j.chembiol.2017.12.014
18. Sha Y, Liu W, Wei X, Zhu X, Luo X, Liang L, Guo T. (2019). Biallelic mutations in Sperm flagellum 2 cause human multiple morphological abnormalities of the sperm flagella (MMAF) phenotype. https://doi.org/10.1111/cge.13602
19. Alfred SE, Surendra A, Le C, Lin K, Mok A, Wallace IM, Proctor M, Urbanus ML, Giaever G, Nislow C. (2012). A phenotypic screening platform to identify small molecule modulators of Chlamydomonas reinhardtiigrowth, motility and photosynthesis. https://doi.org/10.1186/gb-2012-13-11-r105
20. Wu H, Liu Y, Li Y, Li K, Xu C, Gao Y, Lv M, Guo R, Xu Y, Zhou P, Wei Z, Hua R, He X, Cao Y. (2023). DNALI1 deficiency causes male infertility with severe asthenozoospermia in humans and mice by disrupting the assembly of the flagellar inner dynein arms and fibrous sheath. https://doi.org/10.1038/s41419-023-05653-y
21. Avasthi P, Marley A, Lin H, Gregori-Puigjane E, Shoichet BK, von Zastrow M, Marshall WF. (2012). A Chemical Screen Identifies Class A G-Protein Coupled Receptors As Regulators of Cilia. https://doi.org/10.1021/cb200349v

22. Sironen A, Kotaja N, Mulhern H, Wyatt TA, Sisson JH, Pavlik JA, Miiluniemi M, Fleming MD, Lee L. (2011). Loss of SPEF2 Function in Mice Results in Spermatogenesis Defects and Primary Ciliary Dyskinesia1. https://doi.org/10.1095/biolreprod.111.091132

23. Braverman B, Mets DG, York R. (2024). The phenotype-o-mat: A flexible tool for collecting visual phenotypes. https://doi.org/10.57844/arcadia-112f-5023

24. Yap YT, Li W, Huang Q, Zhou Q, Zhang D, Sheng Y, Mladenovic-Lucas L, Yee S-P, Orwig KE, Granneman JG, Williams DC, Hess RA, Toure A, Zhang Z. (2023). DNALI1 interacts with the MEIG1/PACRG complex within the manchette and is required for proper sperm flagellum assembly in mice. https://doi.org/10.7554/elife.79620

25. Virtanen P, Gommers R, Oliphant TE, Haberland M, Reddy T, Cournapeau D, Burovski E, Peterson P, Weckesser W, Bright J, van der Walt SJ, Brett M, Wilson J, Millman KJ, Mayorov N, Nelson ARJ, Jones E, Kern R, Larson E, Carey CJ, Polat İ, Feng Y, Moore EW, VanderPlas J, Laxalde D, Perktold J, Cimrman R, Henriksen I, Quintero EA, Harris CR, Archibald AM, Ribeiro AH, Pedregosa F, van Mulbregt P, Contributors S1, Vijaykumar A, Bardelli AP, Rothberg A, Hilboll A, Kloeckner A, Scopatz A, Lee A, Rokem A, Woods CN, Fulton C, Masson C, Häggström C, Fitzgerald C, Nicholson DA, Hagen DR, Pasechnik DV, Olivetti E, Martin E, Wieser E, Silva F, Lenders F, Wilhelm F, Young G, Price GA, Ingold G-L, Allen GE, Lee GR, Audren H, Probst I, Dietrich JP, Silterra J, Webber JT, Slavič J, Nothman J, Buchner J, Kulick J, Schönberger JL, de Miranda Cardoso JV, Reimer J, Harrington J, Rodríguez JLC, Nunez-Iglesias J, Kuczynski J, Tritz K, Thoma M, Newville M, Kümmerer M, Bolingbroke M, Tartre M, Pak M, Smith NJ, Nowaczyk N, Shebanov N, Pavlyk O, Brodtkorb PA, Lee P, McGibbon RT, Feldbauer R, Lewis S, Tygier S, Sievert S, Vigna S, Peterson S, More S, Pudlik T, Oshima T, Pingel TJ, Robitaille TP, Spura T, Jones TR, Cera T, Leslie T, Zito T, Krauss T, Upadhyay U, Halchenko YO, Vázquez-Baeza Y. (2020). SciPy 1.0: fundamental algorithms for scientific computing in Python. https://doi.org/10.1038/s41592-019-0686-2

26. Lehti MS, Zhang F-P, Kotaja N, Sironen A. (2017). SPEF2 functions in microtubule-mediated transport in elongating spermatids to ensure proper male germ cell differentiation. https://doi.org/10.1242/dev.152108

27. Seabold S, Perktold J. (2010). Statsmodels: Econometric and Statistical Modeling with Python. https://doi.org/10.25080/majora-92bf1922-011

28. Silflow CD, Lefebvre PA. (2001). Assembly and Motility of Eukaryotic Cilia and Flagella. Lessons fromChlamydomonas reinhardtii. https://doi.org/10.1104/pp.010807

29. Terpilowski M. (2019). scikit-posthocs: Pairwise multiple comparison tests in Python. https://doi.org/10.21105/joss.01169

30. Ulicna K, Vallardi G, Charras G, Lowe AR. (2021). Automated Deep Lineage Tree Analysis Using a Bayesian Single Cell Tracking Approach. https://doi.org/10.3389/fcomp.2021.734559

31. Scott DW. (1992). Multivariate Density Estimation. https://doi.org/10.1002/9780470316849

32. https://jmlr.csail.mit.edu/papers/v12/pedregosa11a.html

33. Braverman B. (2024). Building a phenotype-o-mat: A low-cost DIY plate reader for high-throughput phenotype measurements v1. https://doi.org/10.17504/protocols.io.yxmvm3r3ol3p/v1

34. Liu Q, Xu C, Kirubakaran S, Zhang X, Hur W, Liu Y, Kwiatkowski NP, Wang J, Westover KD, Gao P, Ercan D, Niepel M, Thoreen CC, Kang SA, Patricelli MP, Wang Y, Tupper T, Altabef A, Kawamura H, Held KD, Chou DM, Elledge SJ, Janne PA, Wong K-K, Sabatini DM, Gray NS. (2013). Characterization of Torin2, an ATP-Competitive Inhibitor of mTOR, ATM, and ATR. https://doi.org/10.1158/0008-5472.can-12-1702

35. Ahmed M, Hussain AR, Bavi P, Ahmed SO, AlSobhi SS, Al-Dayel F, Uddin S, Al-Kuraya KS. (2014). High prevalence of mTOR complex activity can be targeted using Torin2 in papillary thyroid carcinoma. https://doi.org/10.1093/carcin/bgu051

36. Hanson KK, Ressurreição AS, Buchholz K, Prudêncio M, Herman-Ornelas JD, Rebelo M, Beatty WL, Wirth DF, Hänscheid T, Moreira R, Marti M, Mota MM. (2013). Torins are potent antimalarials that block replenishment of Plasmodium liver stage parasitophorous vacuole membrane proteins. https://doi.org/10.1073/pnas.1306097110

37. Montané M-H, Menand B. (2019). TOR inhibitors: from mammalian outcomes to pharmacogenetics in plants and algae. https://doi.org/10.1093/jxb/erz053

38. Furuta A, Yagi T, Yanagisawa H-a, Higuchi H, Kamiya R. (2009). Systematic Comparison of in Vitro Motile Properties between Chlamydomonas Wild-type and Mutant Outer Arm Dyneins Each Lacking One of the Three Heavy Chains. https://doi.org/10.1074/jbc.m807830200

39. Shitanda I, Tanaka K, Hoshi Y, Itagaki M. (2014). Electrochemical monitoring systems of demembranated flagellate algal motility for ATP sensing. https://doi.org/10.1039/c3an01678a

40. Kamiya R. (2000). Analysis of Cell Vibration for Assessing Axonemal Motility in Chlamydomonas. https://doi.org/10.1006/meth.2000.1090

41. Guo J, Worden A, Hartzog G, Manuel Ares a. (2017). Plasmid DNAs designed for expression in Micromonas CCMP1545 v1. https://doi.org/10.17504/protocols.io.i9wch7e

42. Manton I, Parke M. (1960). Further observations on small green flagellates with special reference to possible relatives of Chromulina pusilla Butcher. https://doi.org/10.1017/s0025315400013321

43. Butcher RW. (1952). Contributions to our knowledge of the smaller marine algae. https://doi.org/10.1017/s0025315400003751